IMEKO 20th TC3, 3rd TC16 and 1st TC22 International Conference
Cultivating metrological knowledge
27th to 30th November, 2007. Merida, Mexico.

Characterization of the imgc-dh100l pressure balance using finite element analysis

G. Buonanno◊ , J. Man□, G. Molinar Min Beciet☼

◊ Di.M.S.A.T. – University of Cassino (Italy)
□ National Measurement Institute, PO Box 264, Lindfield NSW 2070 (Australia)
☼ I.N.RI.M. – Torino (Italy)

Abstract

The National Measurement Institute of Australia (NMIA) and the Istituto Nazionale di Ricerca Metrologia of Italy together with the University of Cassino (INRIM/UNICAS) have participated in a research project to characterise a INRIM 100 MPa free deformation piston and cylinder assembly using two different numerical procedures based on a finite element method (FEM). The pressure distortion coefficient, λ and the piston fall rates, *v* were calculated from the clearance profile between the piston and cylinder obtained from dimensional measurement data. Comparison of the numerical results obtained by the two groups showed a relative difference of 2×10^{-4} in λ and 2.5×10^{-2} in *v*. The numerical results were also compared to the experimental results with a relative difference of 1.9 % in λ and 16 % at 100 MPa in *v*. This paper presents the numerical model used for the calculations of the pressure distortion coefficient and the piston fall rates with a sensitivity analysis of the model for the estimation of the uncertainty values of these two parameters.

Keywords: Finite element method (FEM), pressure balance, pressure distortion coefficient

1. Introduction

The pressure distortion coefficient, λ, and the piston fall-rate, *v*, are important parameters for the characterisation of pressure balances especially when operating at high pressures [1-3]. These parameters depend on the design of a piston-cylinder assembly and on the operating conditions. Because of the complexity of the geometry of a piston-cylinder assembly and of the boundary conditions, numerical procedures based on finite element methods (FEM) are commonly applied to solve the mechanical theory of equations of elastic equilibrium. In the last few years, many authors have used FEM to characterise and to design pressure balances and, in particular, to evaluate the pressure distortion coefficient. [5-8]. These authors used a “iterative method" to evaluate λ, based on the combined analysis of the laminar flux of the pressure transmitting fluid in the clearance and the elastic distortions of the piston and cylinder unit. Workers at the Italian National Research Institute of Metrology and the University of Cassino (INRIM/UNICAS) and the National Measurement Institute of Australia (NMIA) have carried out the characterisation of an INRIM 100 MPa free deformation pressure balance (IMGC-DH100L) using two different numerical procedures and experimental data. This paper presents the

numerical model with a sensitivity analysis of the model. The difference in the calculated values of λ reported by the two groups as well as their associated uncertainties can be considered as a measure of the possible errors in determining the distortion coefficients using a Finite Element Method. The numerical results are compared with the experimental values and their comparison is discussed.

2. Design and properties of the assembly

The pressure balance under investigation is IMGC-DH100L, manufactured by *Budenberg-Desgranges et Huot* (DH), France. The piston-cylinder unit, made of tungsten carbide, has a total engagement length of 26.10 mm. The pressure medium fluid is di-ethyl-hexyl-sebacate. Table I presents the material properties of the piston-cylinder unit and the fluid properties of di-ethyl-hexyl-sebacate that are required for the numerical calculations.

Tab. I – Material and fluid properties.

Property	Value
Measurement range/MPa	Up to 100
Piston Young modulus (tungsten carbide 10 % Co)/GPa	620
Cylinder Young modulus (tungsten carbide 10 % Co)/GPa	620
Piston and cylinder Poisson ratio	0.218
Working fluid	di-ethyl-hexyl-sebacate
Density/kg m^{-3} at 20°C up to 500 MPa	$\rho = 912.6657 + 0.752097 \cdot p - 1.64485 \cdot 10^{-3} \cdot p^2 + 1.45625 \cdot 10^{-6} \cdot p^3$
Dynamic viscosity/Pa s at 20°C up to 500 MPa	$\eta = 0.021554 \cdot (1 + 1.90036 \cdot 10^{-3} \cdot p)^{8.8101}$

Evaluation of the IMGC-DH100L piston-cylinder unit was carried out with the following hypotheses:

i) the radial dimension of the undistorted clearance between the piston and cylinder is based on the dimensional measurements along the engagement length in the axial direction;

ii) axisymmetric geometry model;

iii) rotation of the piston and its frictional effects are not considered.

Assuming the piston cylinder assembly to be axially symmetric, it is possible to simplify the geometry model by means of a radial section as shown in Fig. 1 with coordinates of the main points used in the model shown in Tab. II.

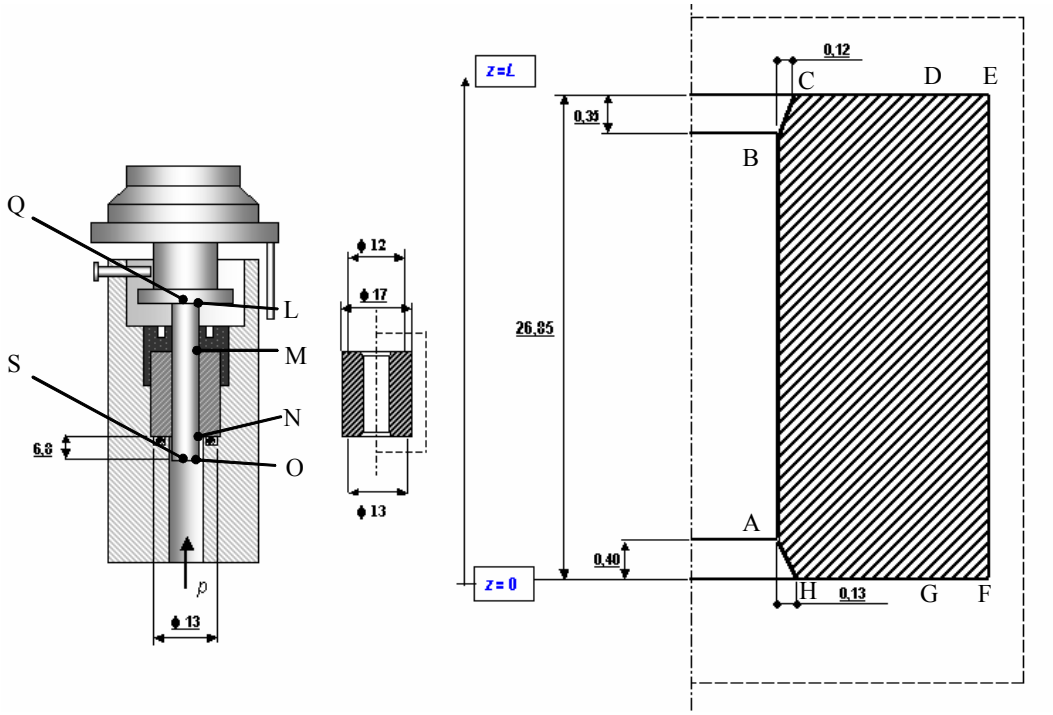

Fig. 1 – Simplified geometrical model adopted in the present calculations (All dimensions in mm)

Tab. II – Coordinates of the main points for the piston and cylinder
(*)=dimensional data

Point	***r* coordinate/mm**	**z coordinate/mm**
H	1.8973	0.00
A	1.7672 (*)	0.40
B	1.7672 (*)	26.50
C	1.8872	26.85
D	6.0000	26.85
E	8.5000	26.85
F	8.5000	0.00
G	6.5000	0.00
Point	***r* coordinate/mm**	**z coordinate/mm**
Q	0.00	36.85
L	1.7666	36.85
M	1.7666 (*)	26.85
N	1.7666 (*)	0.00
O	1.7666	-6.80
S	0.00	-6.80

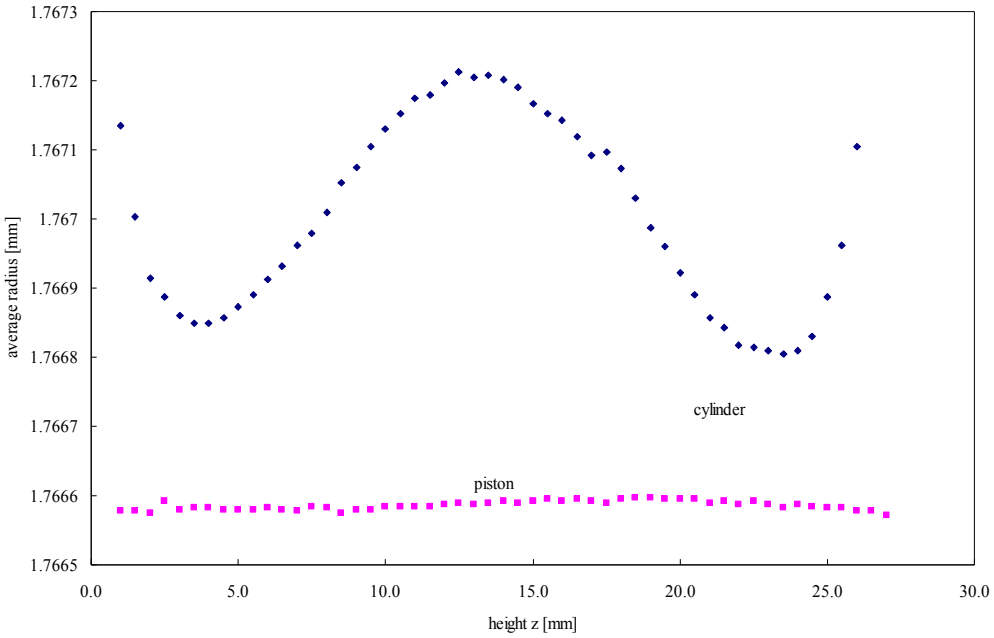

Fig. 2 – Undistorted average radii of the cylinder and piston

The average radii of the piston and cylinder over the engagement length are reported in Fig. 2. These results were obtained using two diameter measurements at right angles of the piston and cylinder bore (*d* and *D* respectively) at three values of z as reference points for converting the straightness data, obtained along four different generatrices, to a series of radii based on straight, hypothetical axes. The expanded uncertainties of the diameter measurements are reported as 80 nm for both the piston and cylinder.

The expanded uncertainty associated with the straightness measurement results is 50 nm. Workers at INRIM have verified the congruence of the diameter measurement results and the straightness measurements results and reported the standard uncertainties of the average radii of the piston and cylinder shown in figure 2 as $U(r)$ = 25 nm and $U(R)$ = 25 nm respectively.

The peculiar shape of the cylinder provides an interesting possibility for studying its influence on the main parameters that characterise a pressure balance.

3. Methods of distortion calculation

The elastic distortions of the piston and cylinder at a given pressure can be calculated using equations of elastic equilibrium if the pressure distribution of the pressure transmitting fluid in the clearance between the piston and cylinder is known. However, calculation of the pressure distribution in the clearance based on a one-dimensional, viscous and laminar flow model requires data of the piston-cylinder distortions. NMIA and INRIM/UNICAS applied different iteration procedures to solve the interdependence of the piston and cylinder distortion calculations and the pressure profile calculations. Initially, a linear pressure profile in the clearance is assumed and the distortions of the piston and cylinder are obtained by solving the equations of elastic equilibrium using a

Finite Element Method (FEM) [3]. This clearance profile is used to calculate a new pressure profile in the clearance. The elastic distortion and fluid flow calculations are repeated until convergence of the output parameters of interest is reached. NMIA compared the pressure distribution in the clearance obtained from one iteration to the next until the convergence criterion $(p_i - p_{i-1})/p_m < 10^{-6}$ was reached, where *i* is the iteration step index and p_m is the applied pressure. INRIM/UNICAS compared the effective area, $A_{e,i}$ obtained from one iteration to the next until the relative difference was smaller than 10^{-9}.

The effective area for a piston-cylinder assembly, A_e in its distorted configuration may be expressed [9] by balancing the axial forces acting on the piston:

$$A_e = \pi r_p^2 \left[1 + 2\frac{u(z_m)}{r_p}\right] + \frac{2\pi}{p_m}\int_{z_m}^{z_a} r(z)\left(-\frac{h(z)}{2}\frac{dp}{dz}\right)dz + \frac{2\pi}{p_m}\int_{z_m}^{z_a} r(z)\left(p(z)\frac{dr}{dz}\right)dz \qquad (1)$$

where r_p is the undistorted piston radius at z_m, $u(z_m)$ is the piston displacement at z_m and $r(z)$ is the distorted piston radius. In general, the effective area varies linearly with the applied pressure for a free deformation piston-cylinder assembly, and the relationship between A_e and P_m may be expressed as the following [10]:

$$A_e = A_0(1 + \lambda P_m) \qquad (2)$$

where A_0 is the effective area at the reference temperature (in our case 20 °C) and atmospheric pressure and λ is the pressure distortion coefficient. These values can be evaluated by fitting the values of A_e versus P_m. Alternatively; A_0 can be calculated using the undistorted clearance profile based on equations expressed in Dadson *et a*l. [1].

The fall rate of the piston can be numerically evaluated as:

$$v = \frac{\dot{m}}{\pi\rho(p)r_p^2}\,. \qquad (3)$$

where $\dot{m}$ is the mass flow rate. The boundary conditions to solve the system of differential equations, in relation to the geometric domain reported in Fig. 1 are:

Cylinder boundary conditions

1) $p(r,z) = p(z)$ for each (r,z) belonging to $\overline{\mathrm{HA}}$ and $\overline{\mathrm{AB}}$ and $\overline{\mathrm{BC}}$
2) $p(r,\mathrm{z}) = p_\mathrm{a}$ for each (r,z) belonging to $\overline{\mathrm{CD}}$ and $\overline{\mathrm{EF}}$
3) $p(r,\mathrm{z}) = p_\mathrm{m}$ for each (r,z) belonging to $\overline{\mathrm{GH}}$
4) $\mathrm{w}(r,\mathrm{z}) = 0$ for each (r,z) belonging to $\overline{\mathrm{DE}}$ and $\overline{\mathrm{FG}}$

Piston boundary conditions

1) $p(r,\mathrm{z}) = p_\mathrm{m}$ for each (r,z) belonging to $\overline{\mathrm{NO}}$ and $\overline{\mathrm{OS}}$
2) $p(r,\mathrm{z}) = p_\mathrm{a}$ for each (r,z) belonging to $\overline{\mathrm{LM}}$

3) $p(r,z) = p(z)$ for each (r,z) belonging to $\overline{MN}$

4) $u(r,z) = 0$ for each (r,z) belonging to $\overline{QS}$

5) $w(r,z) = 0$ for each (r,z) belonging to $\overline{QL}$

where $p(z)$ is the pressure in the clearance along the engagement length; p_a is the ambient pressure; p_m is the applied pressure; $w(r,z)$ is the displacement in the *z*-direction and $u(r,z)$ is the displacement in *r*-direction.

Both NMIA and the INRIM/UNICAS used different FEM software to solve the equations of elastic equilibrium. INRIM/UNICAS applied the multipurpose finite element software FEMLAB 2.3 ®, by running the FEM model from the Matlab ® prompt. Matlab subroutines developed in-house were used to compute the iterative procedure. These subroutines had been validated by comparing the present results with previous results obtained in [5-7]. The computational domain in the geometry model was meshed by means of linear triangular elements. The shape of the triangular elements can greatly influence the FEA because excessively distorted elements will cause errors in the numerical solutions. The number of nodes along the clearance was 260 for the piston and 261 for the cylinder. These numbers were chosen on the basis of sensitivity analysis and were considered to be an optimum choice between computational time and accuracy of the solution.

The NMIA utilised the ANSYS FE program to calculate the elastic deformations of the IMGC-DH100L piston and cylinder unit. The geometry model was meshed using 8-node quadrilateral elements. The line between two key points was divided into segments for controlling the meshing size. A number of segments along the clearance for the IMGC-DH100L unit were used to examine the effect of the element size on the effective area of the piston-cylinder unit calculated from FEA results. It is found that the relative change in A_e is less than 0.05 ppm when the number of nodes is increased 50% from 1045 to 1567 nodes but the computing time usage is 17 minutes and 44 minutes respectively for obtaining the solution. It was decided to use 1045 nodes for the FEA analysis.

Numerical results and discussion

Calculations were performed for pressures of 10, 25, 50, 75, 100 MPa at a reference temperature of 20 °C by NMIA and INRIM/UNICAS. A plot of the dimensionless pressure p^* in the clearance ($p^* = (p(z) - p_a)/p_m$), the radial displacements of the piston $u/\mu m$ and of the cylinder $U/\mu m$ in the clearance versus the dimensionless coordinate z^* (referred to the axial length of the clearance, $z^* = 0$ at $z = z_m = 0.40$ mm and $z^* = 1$ at $z = z_a = 26.50$ mm) for three different applied pressures are presented in Figure 3.

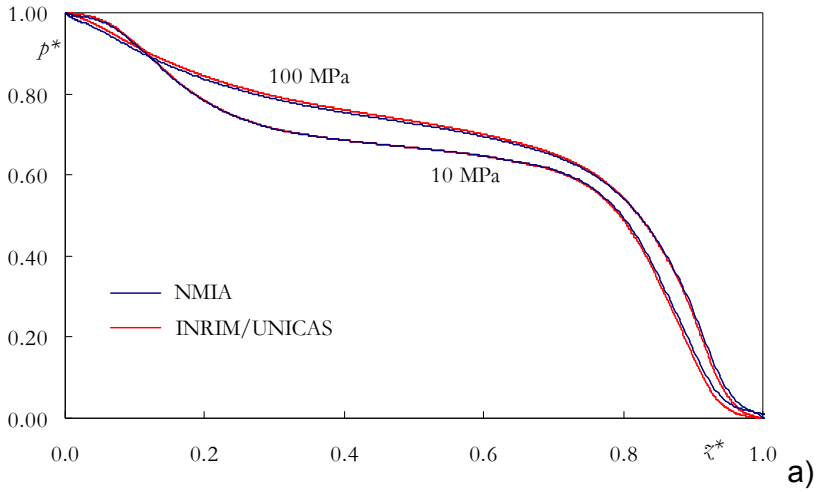

a)

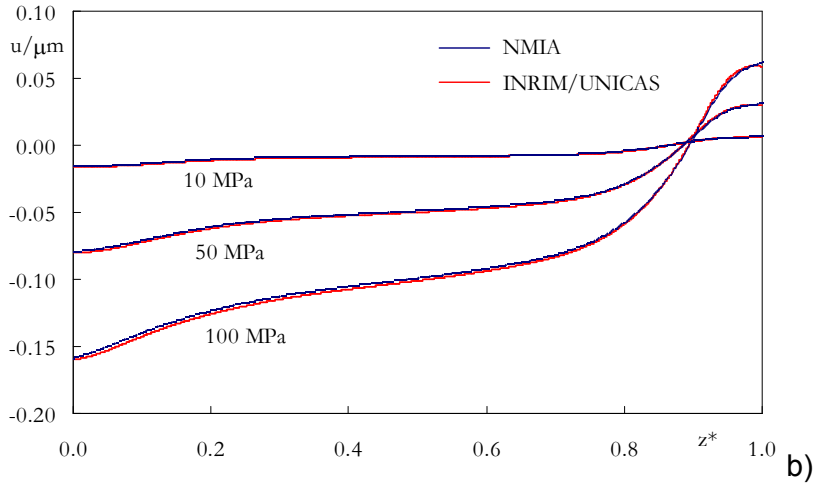

b)

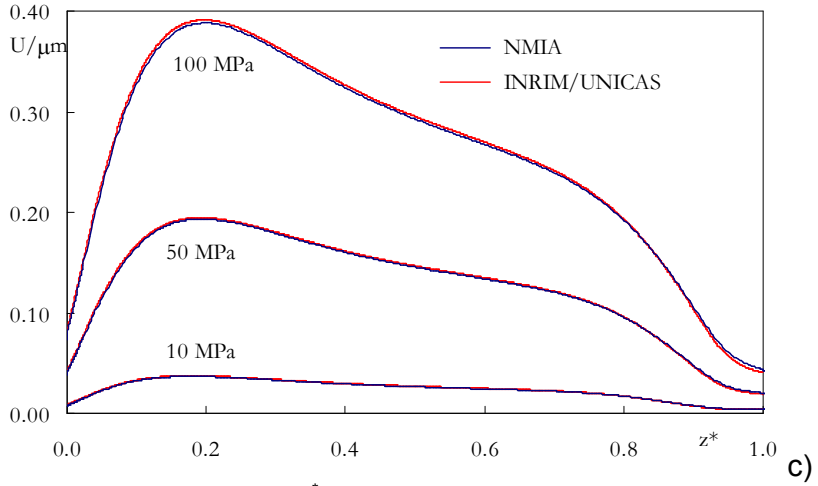

c)

Fig. 3 - Dimensionless pressure p^*, radial displacements of the piston, u and cylinder U in the clearance versus normalised axial coordinate z^*

From figure 3, it can be noted that:

- the numerical results obtained by NMIA and INRIM/UNICAS using different numerical procedures are in excellent agreement;
- the shape of the dimensionless pressure p^* depends on the applied pressure;
- the radial distortions of the cylinder show a maximum value at $z^* \approx 0.2$, for all the three applied pressures. It is of interests noting that the shape of the cylinder radii profile gives always a maximum at $z^* \approx 0.2$.

The numerical results were used to calculate the effective area, A_e using equation (1) and the piston fall rate using equation (3). The pressure distortion coefficient, λ and the values of the effective area at atmospheric pressure and at 20 °C, A_o were determined by fitting the values of A_e versus P_m using equation (2). The values of λ and A_o obtained by numerical calculations together with the experimental results are reported in Tab. III.

Tab. III – Distortion coefficient λ and effective area, A_o at reference conditions.

	INRIM/UNICAS	*NMIA*	*Experimental*
λ / *MPa*$^{-1}$	9.32×10^{-7}	9.32×10^{-7}	9.50×10^{-7}
A_0 / *mm*^{2}	9.806042	9.806029	9.806227

It can be seen that the difference between the calculated values of pressure distortion coefficient obtained by INRIM/UNICAS and NMIA is 0.02%, whereas the difference between the numerical and the experimental result is 1.9 %. This difference falls within the 3 % uncertainty of the measurement result. The numerical value of the effective area, A_o obtained by INRIM/UNICAS is in excellent agreement (1.6 ppm) to the theoretical value obtained by applying the Dadson equation [1]. This comparison provides a check of the FEA procedure.

The numerical value of A_o obtained by NMIA agrees within 3 ppm with those reported by INRIM/UNICAS. The difference between the experimental value and the numerical values is 19 ppm, which is within the expanded uncertainty associated with the experimental value of A_o of 23 ppm. However, there is a need to find out the reasons for this difference.

The calculated piston fall-rate values and the experimental values obtained at (21.7 ± 0.2) °C are plotted versus pressure in Fig. 4. It is seen that the agreement between the numerical values obtained by INRIM/UNICAS and NMIA is within 2.5%, and the theoretical values fall within the uncertainty of the experimental values at lower pressures. However at 100 MPa, the measured and theoretical fall rate values are 1.84 μm/s and 1.55 μm/s respectively giving a difference of 16%. This difference could be a result of uncertainties in the fluid flow model and some other effects such as temperature drift during the measurement.

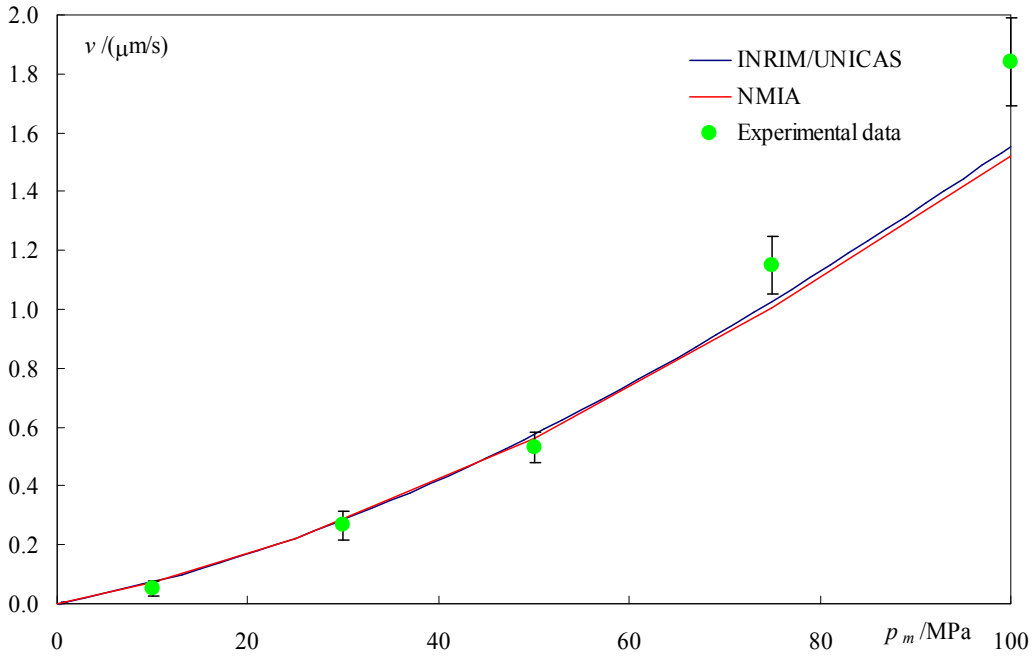

Fig. 4 – A plot of piston fall rate versus pressure

4. Uncertainty analysis of the numerical model

The standard uncertainties of the pressure distortion coefficient and of the piston fall rate resulting from FEM modelling calculations are evaluated by considering the standard uncertainties of the input quantities to the numerical model. The input quantities considered are the Young's Modulus and Poisson ratio of the piston and cylinder units (E_p, E_c, μ_p, μ_c), gap shape (conical convergent and divergent), the undistorted gap width. The working fluid density and viscosity properties are not included in this analysis as their uncertainty contributions are usually negligible [2].

The standard uncertainty of λ due to the uncertainty contribution of an input quantity, $u(x_i)$, is $\left(\partial\lambda/\partial x_i\right)\cdot u\left(x_i\right)$, where $\left(\partial\lambda/\partial x_i\right)$ is the sensitivity coefficient of the input quantity. The sensitivity coefficient can be evaluated based on a finite difference approach [11]. The authors used FEM procedures to calculate the change of λ with a small variation in each input quantity at an applied pressure of 100 MPa and reference temperature of 20 °C. The gap shape variation was generated by varying the cylindrical radial gap profile within ±0.1 μm giving a mean radial gap of the same value as the original cylinder gap profile. This was achieved by rotating the line AB (see Fig. 1) with respect to the centre of the engagement length along the *r* axis. A convergent gap profile moved point B -0.1 μm and point A +0.1 μm. These values were reversed for a divergent gap profile. Based on this analysis, Table IV reports the sensitivity coefficient values and the uncertainty contribution of the input quantities to the calculated pressure distortion coefficient. Table V presents the uncertainty analysis of the numerical piston fall rate calculated at a pressure of 100 MPa.

Table IV. Uncertainty analysis of the calculated pressure distortion coefficient ($\lambda = 9.32\times10^{-7}$ MPa^{-1})

Quantity	**Standard uncertainty**	**Sensitivity coefficient** $\frac{\partial\lambda}{\partial x_i}$		**Relative standard uncertainty** $u(\lambda)/\lambda \times 10^2$	
x_i	$u(x_i)$	*INRIM/UNICAS*	*NMIA*	*INRIM/ UNICAS*	*NMIA*
E_p=6.2×10^5 MPa	31×10^3 MPa	4.11×10^{-13} MPa^{-2}	3.88×10^{-13} MPa^{-2}	1.4	1.3
E_c=6.2×10^5 MPa	31×10^3 MPa	-1.86×10^{-12} MPa^{-2}	-1.40×10^{-12} MPa^{-2}	6.2	4.6
μ_p= 0.218	1.1×10^{-2}	2.13×10^{-6} MPa^{-1}	2.15×10^{-6} MPa^{-1}	2.5	2.5
μ_c = 0.218	1.1×10^{-2}	1.01×10^{-6} MPa^{-1}	1.00×10^{-6} MPa^{-1}	1.2	1.2
Quantity	**Standard uncertainty**	**Standard uncertainty** $u(\lambda)$ / 10^{-6} MPa^{-1}		**Relative standard uncertainty** $u(\lambda)/\lambda \times 10^2$	
x_i	$u(x_i)$	*INRIM/UNICAS*	*NMIA*	*INRIM/ UNICAS*	*NMIA*
Gap width	+ 0.1 μm	-4.6×10^{-2}	-5.0×10^{-2}	-4.9	-5.0
	– 0.1 μm	8.7×10^{-2}	1.05×10^{-1}	9.3	11.3
Gap shape	0.1 μm/13.05 mm (convergent)	1.7×10^{-1}	1.8×10^{-1}	18	19
	0.1 μm/13.05 mm (divergent)	2.7×10^{-1}	2.5×10^{-1}	29	27

Table V. Uncertainty analysis of the numerical piston fall rate value at 100 MPa. (v = 1.55 μm/s)

Quantity	**Standard uncertainty**	**Sensitivity coefficient** $\frac{\partial v}{\partial x_i}$		**Relative standard uncertainty** $u(v)/v \times 10^2$	
x_i	$u(x_i)$	*INRIM/UNICAS*	*NMIA*	*INRIM/ UNICAS*	*NMIA*
E_p=6.2×10^5 MPa	31×10^3 MPa	-7.80×10^{-7} μm s^{-1} MPa^{-1}	-7.73×10^{-7} μm s^{-1} MPa^{-1}	1.5	1.5
E_c=6.2×10^5 MPa	31×10^3 MPa	-2.66×10^{-6} μm s^{-1} MPa^{-1}	-3.29×10^{-6} μm s^{-1} MPa^{-1}	5.3	6.5
μ_p= 0.218	1.1×10^{-2}	-3.54 μm s^{-1}	-3.48 μm s^{-1}	2.5	2.5
μ_c = 0.218	1.1×10^{-2}	1.42 μm s^{-1}	1.39 μm s^{-1}	1.0	1.0
Quantity	**Standard uncertainty**	**Standard uncertainty** $u(v)$ / μm s^{-1}		**Relative standard uncertainty** $u(v)/v \times 10^2$	
x_i	$u(x_i)$	*INRIM/UNICAS*	*NMIA*	*INRIM/ UNICAS*	*NMIA*
Gap width	+ 0.1 μm – 0.1 μm	9.6×10^{-1} -7.0×10^{-1}	9.4×10^{-1} -6.5×10^{-1}	61.9 -45.2	60.6 -41.9
Gap shape	0.1 μm/13.05 mm (convergent)	-3.1×10^{-1}	-3.0×10^{-1}	-20.0	-19.4
	0.1 μm/13.05 mm (divergent)	1.8×10^{-1}	1.5×10^{-1}	11.6	9.7

From Table IV, It is seen that an estimated uncertainty of 5% in the Young's modulus and in the Poisson ratio of the piston and cylinder material contributes a relative standard uncertainty of λ from 1.2% to 6.2%, with the largest contribution due to the Young's modulus of the cylinder. Particular attention should therefore be paid to reduce the measurement uncertainty of the Young modulus of the cylinder. The sensitivity coefficient values obtained for the Young's modulus and Poisson ratio in this analysis are similar in magnitudes to those determined by the authors in previous FEA modelling work. A variation of the undistorted gap width of +0.1 μm gives rise to a relative uncertainty of λ of 4.9 % obtained by INRIM/UNICAS and 5.0 % by NMIA. In the case of a variation of the gap width of -0.1 μm, the respective relative uncertainty of λ is 9.3 % and 11.3%. It seems that the effect of the variation of gap width on the distortion coefficient exhibits a non linear behaviour producing a larger uncertainty value of λ with a decrease in gap width. The gap shape variation has a very significant contribution on λ uncertainty, giving rise to a relative uncertainty of 19% for a convergent gap shape and 29% for a divergent one.

From Table V, it is observed an estimated uncertainty of 5% in the Young's modulus and in the Poisson ratio of the piston and cylinder material gives rise to a relative standard uncertainty of the piston fall rate of 1.0 % to 6.5%, with the largest contribution due to the Young's modulus of the cylinder. The gap width parameter has a great influence on the piston fall rate. An increase of 0.1μm of the gap width would produce a relative standard uncertainty of 60.6 % to 61.9 % as obtained by NMIA and INRIM/UNICAS respectively whilst a decrease of 0.1 μm in the gap width gives rise to 41.9% and 45.2 %. Variation in the gap shape of a conical convergent profile gives a relative uncertainty of the piston fall rate of 20% and the divergent profile gives 11.6% and 9.7% obtained by INRIM/UNICAS and NMIA respectively. This analysis shows that the piston fall rate is very sensitive to the gap width and the gap shape.

5. Conclusions

NMIA and the INRIM/UNICAS have calculated the effective area A_o, the distortion coefficient, λ and the piston fall rate, v of the 100 MPa IMGC-DH100L free deformation unit, in liquid media, using different FEA procedures. The respective values for A_0 are 9.806029 mm^2 and 9.806042 mm^2; and for λ are 9.32×10^{-7} MPa^{-1} and 9.32×10^{-7} MPa^{-1}. Comparison of these results shows a relative difference of 3×10^{-6} in A_o and 2×10^{-4} in λ. A comparison of the theoretical values with the experimental values indicate a relative difference of 1.9×10^{-5} in A_o and 2.0×10^{-2} in λ. These differences fall within the uncertainty of the measurement values. The sensitivity analysis of the input quantities for calculating the pressure distortion coefficient indicates that the variation of the gap shape geometry as conical convergent has the largest effect on λ. This variation has been taken as the uncertainty contribution of the inclination of the piston and cylinder generatrices. The combined standard uncertainty values associated with the calculated pressure distortion coefficient are estimated as 2.9×10^{-7} MPa^{-1} (31%) and 2.7×10^{-7} MPa^{-1} (29%) by NMIA and INRIM/UNICAS respectively. The numerical values of piston fall rate reported by NMIA and INRIM/UNICAS agree within 2.5%. The numerical values fall within the uncertainty of the measured piston fall rates at lower pressures. At 100 MPa, a difference of 16% is observed between the numerical and experimental values but analysis shows that the fall rate is very sensitive to gap shape and gap width so such difference can be expected. The combined standard uncertainty of the calculated piston fall rate at 100 MPa reported by NMIA and INRIM/UNICAS are 1.03 μm s^{-1} (66 %) and 0.99 μm s^{-1} (64 %) respectively.

References

[1] Dadson R. S., Lewis S.L., Peggs G.N. (1982), *The pressure balance - Theory and practice*, National Physical Laboratory, London: Her Majesty's Stationery Office.

[2] Buonanno G., Ficco, G., Giovinco G., Molinar G., (2007), *Ten years of experience in modelling pressure balances in liquid media up to few GPa*, Editor: University of Cassino (Italy), ISBN: 978-88-8317-037-9

[3] Bignell N. (editor), (2005), *Pressure measurements*, Monograph 7:NMI Technology Transfer Series, Third Edition, © Commonwealth of Australia

[4] Molinar G., Buonanno G, Dell'Isola M., Maghenzani R., Urbanski M., Wisniewski R. (1999), Elastic distortions of a mixed (simple and re-entrant) piston-cylinder unit for pressure measurements up to 2.6 GPa, *Metrologia*, **36**, 585-590.

[5] Molinar G., Buonanno G., Giovinco G., Delajoud P., Haines R., (2005), Effectiveness of finite element calculation methods (FEM) on high performance pressure balances in liquid media up to 200 MPa, *Metrologia*, **42**, 207-211.

[6] Sabuga W., Molinar G., Buonanno G., Esward T., Rabault T., Yagmur L., (2005), Calculation of the distortion coefficient and associated uncertainty of PTB and LNE 1 GPa pressure balances using finite element analysis – EUROMET project 463. *Metrologia*, **42**, 202- 206.

[7] Sabuga W., Molinar G., Buonanno G., Esward T., Legras J.C., Yagmur L., (2006), Finite element method used for calculation of the distortion coefficient and associated uncertainty of a PTB 1 GPa pressure balance – EUROMET project 463. *Metrologia*, **43**, 311-325.

[8] G. Buonanno, M. Dell'Isola and R. Maghenzani, (1999), A finite element analysis of pressure distortion coefficient and piston fall-rate in a simple pressure balance", *Metrologia*, **36**, n. 6, 579-584.

[9] Buonanno G., Dell'Isola M., Iagulli G., Molinar G.F., (1999), A finite element method to evaluate the pressure distortion coefficient in pressure balances, *High Temperatures – High Pressures*, **31,** 131-143.

[10] Pavese F. and Molinar G.F., (1992), *Modern gas-based temperature and pressure measurements*, Plenum Press, New York

[11] ISO GUIDE, 1993, "*Guide to the Expression of Uncertainty in Measurement*," Geneva